Please provide feedback

Please support the ScholarWorks@UMBC repository by emailing scholarworks-group@umbc.edu and telling us what having access to this work means to you and why it's important to you. Thank you.

Linear and Nonlinear Optical Properties
of Quasi-Periodic One-Dimensional Structures

Concita Sibilia[1], Mario Bertolotti[1], Marco Centini[1], Giuseppe D'Aguanno[1],
Michael Scalora[2], Mark J. Bloemer[2], and Charles M. Bowden[2]

[1] INFM at Dipartimento di Energetica, Universita' di Roma "La Sapienza",
   Via Scarpa 16, 00161 Roma, Italy
   `concita.sibilia@uniroma1.it`
[2] AMSAM-RD-WS-ST, U. S. Army Aviation & Missile Research, Development,
   & Engineering Center
   Redstone Arsenal, AL 35898, USA

Abstract. The optical properties of self-similar optical multilayer structures are first discussed for low input intensities, thus allowing the neglect of nonlinear effects. The structures under consideration are obtained by alternating two dielectric layers of different refractive indexes following a fractal set. The triadic Cantor and the Fibonacci sets are considered, and some applications of the field localization properties of these structures are discussed. Nonlinear behavior is also discussed, restricted to third-order nonlinear polarization of the dielectric materials constituting the structures.

1   Introduction

Quasi-periodic structures with two or more incommensurate periods are intermediate between periodic and random media. The interest in quasi-periodic layered media originated in studies of analogous systems in solid-state physics. The problem of the propagation of electrons in one-dimensional quasi-periodic structures has revealed interesting features, such as the presence of localized, critical, and extended states [1,2,3,4]. Theoretical studies have received great impetus from the experimental discovery of a quasi-crystal phase in metallic alloys [5], which was followed by the realization of quasi-periodic superlattice structures [6].

An analogous problem in optics was addressed by *Kohmoto* et al. [7] who studied a one-dimensional quasi-periodic structure involving a stack of dielectric layers arranged in a Fibonacci sequence. The optical system exhibited several advantages over its solid-state counterpart. In solid-state physics, electron–electron and electron–phonon interactions are inevitable. On the other hand, optical experiments are more "pure," since photons do not interact. Moreover, the polarization of light adds new features to the localization problem which is absent in solid-state physics.

It is of interest to investigate the behavior of quasi-periodic structures mainly because of the peculiar aspects of the localization of light inside fractal

structures. Recently, many theoretical studies of one-dimensional (1-D) quasi-periodic structures based on a Fibonacci or a Cantor sequence have been performed [7,8,9,10], and interesting experimental work has been done [8,9]. The properties of the structures studied [6,7,8,9,10] are linked to the properties of self-similar spaces also because of the possibility of weak localization of photons. The treatment is so general that it can be applied to any kind of waves propagating in a self-similar medium. Photons that localize in fractal structures have been named "fractons," and the existence of fracton modes [11] has been experimentally proven for acoustic waves in one-dimensional Cantor composites [12]. In optics, scattering and diffraction from fractal objects have also been recently investigated [13,14,15,16,17,18,19].

Generally speaking, layered, quasi-periodic structures can be classified as a type of photonic band gap (PBG) structure or crystal. Periodic PBG structures have been recently intensively studied theoretically as well as experimentally [20,21,22]. An essential property of photonic crystals is the existence of forbidden frequency bands, from which propagating modes, spontaneous emission, and zero-point fluctuations are all absent. On the other hand, it has been observed that the electrical-field intensity strongly increases near the PBG edges in the frequency domain transmission curves [23]. This is related to a spatial field distribution localized inside the structure. Many possible applications have been envisioned, and devices function because of field localization effects [23]. Field localization in periodic structures has been described through the concept of density of modes (DOM) [24], a quantity that can be derived directly from transmission properties. The density of modes increases sharply if defects are introduced inside the structure or if the structure is arranged in a quasi-periodic geometry [25]. In what follows, we will discuss in more detail the linear and nonlinear optical properties of multilayer structures based on a Fibonacci or a Cantor code [26,27,28].

2   Something about Fractals

The term "fractal" was introduced by *Mandelbrot* [29] to describe geometric objects with no integral dimension. The definition given by Mandelbrot states that a fractal is a self-similar set whose dimension is different from the topological dimension; a self-similar set is an invariant set with respect to a scale change. Self-similar fractals are generated mathematically by a recursive operation of *generators* and *initiators* [29]. A process is defined on an object, named *initiator*. For example in the Koch fractal, the initiator is a line of unit length. A segment of length 1/3 is erased in the middle of the initiator, and an equilateral triangle, without basis, is built on the segment. This operation can be repeated again at the smallest scale: a line of 1/3 is erased again in the middle of each of the four segments. This fractal has a scale factor of 3 (Fig. 1).
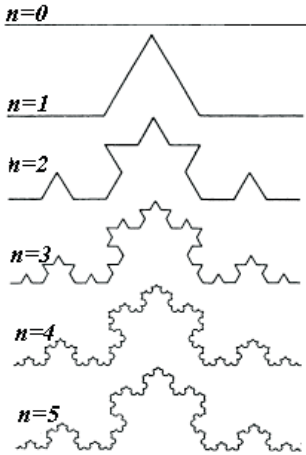
Fig. 1. Example of a self-similar fractal: the Koch fractal

The triadic Cantor set has a generation procedure very similar to the Koch fractal; the difference is that one removes n segments of length $l_n = (1/3)^n$ from an unitary line, without adding any more. We start from a straight line segment of unitary length. Then we "wipe away" the central middle third and repeat the process on the remaining two segments of length $1/3$. Repeating the middle-third wiping-out process over and over again, does not leave a single connected segment. In Fig. 2, the first five levels of the Cantor set generation are shown [10]. The Fibonacci set will be considered later.

The optical structures that we will discuss in the following can be suitably constructed by using the criteria used to define the set. For example, a 1-D structure can be realized with a multilayered stack of different materials assembled following the fractal code.

One of the interesting phenomena appearing in fractal structures of this type is wave localization, so that the field (acoustic, electromagnetic, or other) becomes spatially confined in some suitable regions and/or delocalized in some other parts. Many theoretical papers have been written on this

Fig. 2. Example of the generation sequence of a Cantor set

subject [13,30]. Although the problem originated in solid-state physics in connection with the theory of electrical conductivity in disordered and quasi-periodic media, the subsequent realization that almost any wave equation with a random (or quasi-periodic) potential may possess localized solutions has made the field quite general. We bring forth the analogy to the electronic problem, where localized, extended, and critical states can be defined. Let us recall that by a localized surface wave, or critical states, we mean that the wave functions $\psi(z)$ for the electron or the electrical field optical waves are described by an envelope function that varies asymptotically as $\exp(-\xi z)$ for exponentially localized states, or as $z^{-\xi}$ for a critical state (z is the propagation coordinate). By drawing the analogy to electronic wave functions, one might observe that forbidden bands of energy correspond to almost null transmission in the optics of multilayers; thus, the electrical field distribution is expected to decay exponentially with increasing distance into the structure, producing a "surface localized state." On the contrary, a band of energies corresponding to almost complete transmission is considered an allowed region where "extended states" are likely to be observed. The transition regions therefore correspond to "critical states." Depending on the number of layers and on the spectral width of the associated transmission function, extended states become "bulk localized states." These states appear when the structure has a transmission spectrum that exhibits isolated peaks in the middle of frequency band gaps, and field localization occurs [31]. All of these properties make fractal structures very attractive from the optical point of view, and even more interesting in the framework of their nonlinear response.

One of the most interesting consequences related to the fractal nature of quasi-periodic structures is self-similarity and scaling behavior. Self-similarity and scaling behavior of the transmission spectra in one-dimensional Fibonacci multilayers consisting of quarter-wave plats of SiO_2/TiO_2 were experimentally investigated in [32].

3   Optical Properties of Filters Based on a Fractal Code

Let us consider a structure realized by alternating two dielectric layers of different refractive indexes such that the high-index layers belong to a triadic Cantor set, as described in Figs. 2 and 3. This is obtained by alternating two nondispersive, planar, dielectric layers of refractive indexes n_2 and $n_1(n_2 > n_1)$ whose thicknesses are such that their optical paths are the same. Let us take the layer of refractive index n_2 as the initiator. If L is the optical thickness of the initiator, the generator is obtained by substituting the central part of the initiator, whose optical thickness is $L/3$, with a layer of refractive index n_1 and optical thickness $L/3$. The layered structure is obtained by iterating the operation up and down and stopping the iteration at the Nth step (Fig. 3). For the sake of simplicity, the incident light is assumed
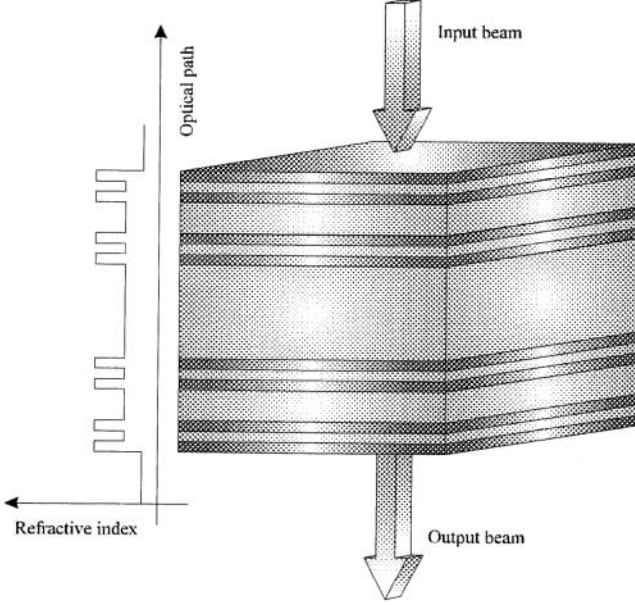
Fig. 3. A layered structure that follows the Cantor set

to be a plane wave propagating in a direction at an angle θ with respect to the normal at the interface planes.

We use the matrix transfer method (see [10] for applications to the Cantor-like multilayer) for calculating the transmission characteristics. The expression of the electrical field transmission (for a linearly polarized wave, parallel to the interface planes of the resonator) at a wavelength λ is as follows

$$t(k_0, L) =$$

$$\frac{2}{T_{22}^{(N)}(k_0, 3^N L) - \frac{T_{21}^{(N)}(k_0, 3^N L)}{i k_0} - i k_0 T_{12}^{(N)}(k_0, 3^N L) + T_{11}^{(N)}(k_0, 3^N L)}, \quad (1)$$

where i is the imaginary unit, k_0 is the vacuum wave number, and $T_{hk}^{(N)}$ are the elements of the transfer matrix $\boldsymbol{T}^{(N)}$ of the structure, obtained by the Nth iteration of the recursive relation, which in Cantor layers is [10]

$$\boldsymbol{T}^{(k)}(3^k \varphi) = \boldsymbol{T}^{(k-1)}(3^{k-1}\varphi)\boldsymbol{T}_1(3^{k-1}\varphi)\boldsymbol{T}^{(k-1)}(3^{k-1}\varphi), \quad k = 1, 2, \ldots, N \quad (2)$$

with

$$\boldsymbol{T}^{(0)}(\varphi) = \boldsymbol{T}_2(\varphi) \tag{3}$$

$$\boldsymbol{T}_h(\varphi) = \begin{pmatrix} \cos\left(\frac{\varphi}{3}\right) & \frac{1}{k_0 n_h}\sin\left(\frac{\varphi}{3}\right) \\ -k_0 n_h \sin\left(\frac{\varphi}{3}\right) & \cos\left(\frac{\varphi}{3}\right) \end{pmatrix}, \quad h = 1, 2, \tag{4}$$
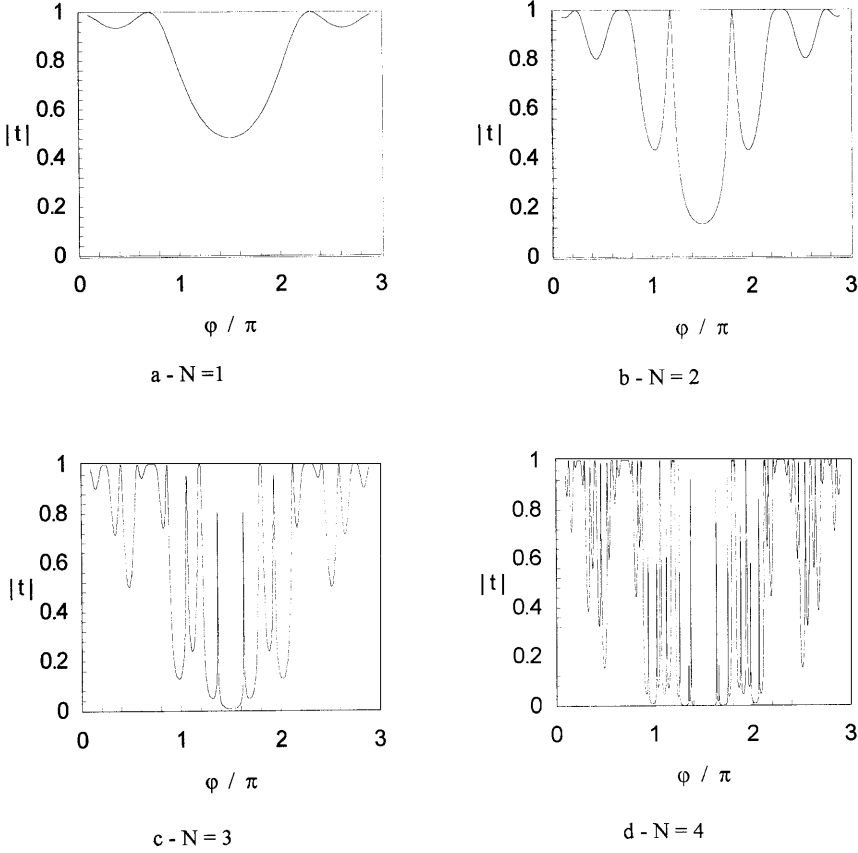
where $\varphi = k_0 L$.

Fig. 4. Examples of transmission spectra as a function of the phase φ for different levels of the Cantor sequence: (a) $N = 1$, (b) $N = 2$, (c) $N = 3$, (d) $N = 4$

Examples of transmission spectra for normal incidence are shown in Fig. 4, where the magnitude of the transmission as a function of φ is given for the first four levels of the Cantor sequence.

Let us consider the spectrum. The electrical field in the layers can either fill the whole structure or can be localized in a smaller region. This different behavior depends on the chosen resonance frequency. If the resonance frequency corresponds to an isolated peak of transmission, then the field is stronger in a selected part of the layered structure. If the resonance frequency corresponds to a broad maximum of the spectrum, then the field exists almost everywhere in the layers. This behavior is shown in Fig. 5a and 5c for $\varphi = 0.7\pi$ and $\varphi = 3\pi$, respectively, which correspond to isolated peaks in the transmission spectrum. If the resonance frequency corresponds to a broad maximum of the spectrum, the field exists almost everywhere in the layered structure, as shown in Fig. 5b, d for $\varphi = 0.7\pi$ and $\varphi = 3\pi$, respectively. Note
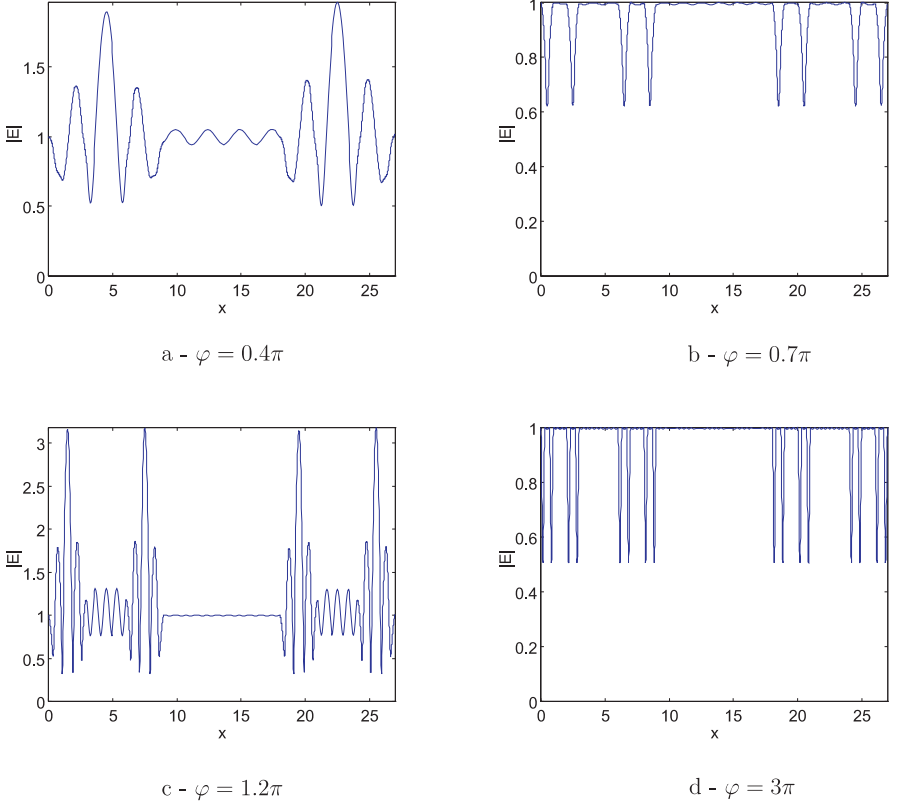
a - $\varphi = 0.4\pi$

b - $\varphi = 0.7\pi$

c - $\varphi = 1.2\pi$

d - $\varphi = 3\pi$

Fig. 5. Electrical field spatial distribution inside the layered Cantor sequences $N = 4$, for different values of φ. ($\varphi_0 = k\lambda$): **(a)** $\varphi = 0.4\pi$; **(b)** $\varphi = 0.7\pi$; **(c)** $\varphi = 1.2\pi$; **(d)** $\varphi = 3\pi$

that the field distribution in Fig. 5d is reminiscent of the structure, as expected. For a Cantor set, the field distribution at the band edge frequency depends on the refractive index of the initiator, in other words, the "central" layer. When the central layer has a low refractive index value, the Cantor set may be considered a resonator with quasi-periodic mirrors, or multiple coupled cavities. For this reason, when we shift the frequency from the low to the high-frequency band edge, the symmetry of the field distribution in the central layer changes.

Similar results can be obtained by using a Fibonacci sequence. An example of a Fibonacci sequence is as follows:

"external medium/ BAABAABAABAABAABABAABABAABAABABAABA/ substrate,"

where each layer has an optical thickness of one-quarter of a wavelength; the symbol A refers to a layer of refractive index n_1, and B refers to a layer of refractive index n_2.

In a Fibonacci multilayer S_j, there are F_j layers given recursively by $F_{j+1} = F_j + F_{j-1}$ (j $\geq$ 1, with $F_0 = A, F_1 = B$).

Transmission properties of such quasi-periodic filters have been discussed in [33] using the method of the "dynamic map", where the 2×2 matrix map can be reduced to a trace map. All of the spectral properties of the layered structures are contained in the properties of the trace map.

Electrical field localization properties in the spatial domain can be derived by spectral analysis of the transmission function. This can done by introducing the concept of the density of modes. The mode density in a *finite* one-dimensional N-period layer stack has been studied analytically in [24], where a correspondence has been found between the group velocity $v = d\omega/dk$ in an *infinite* periodic structure and the density of modes (DOM) $\rho_N = dk_N/d\omega$ of an N-period *finite* 1-D lattice.

The magnitude of the density of modes $\rho(\omega)$ is expressed via the real and imaginary parts of the complex transmission coefficient $t \equiv x + iy \equiv \sqrt{T}e^{i\varphi}$ as follows [24]:

$$\rho(\omega) \equiv \frac{dk}{d\omega} = \frac{1}{D}\frac{y'x - x'y}{x^2 + y^2}, \tag{5}$$

where D is the total physical length of the structure; the prime denotes differentiation with respect to ω. The analytical expression for $\rho(\omega)$ for a quarter-wave, N-period stack composed of two layer unit cells, it has been shown, is many times larger than that for a homogeneous medium. A finite number of unit cells instead of a periodic, infinite structure allows removing the DOM singularity at the band edge and calculating the value of the DOM for practical devices.

The group velocity and DOM are calculated numerically by using (5). Once the group velocity is known, the group index $n_g = c/v_N$ is also evaluated. To show the main features of fractal structures, we may discuss the following: (a) an N-period stack, (b) a Cantor-like multilayer and (c) a Fibonacci multilayer (see Fig. 6). The Cantor-like multilayer is generated by a material having refractive index $n_1 = 2.5$ (initiator). The central part of the initiator is then replaced with a layer of refractive index $n_2 = 1.5$, according to the law of triadic Cantor construction, such that $1/3$ of the generator has the same optical path $L_{opt} = \lambda_0/4$ [25]. Thus, the generator thicknesses are $a = \lambda_0/(4n_1)$ and $b = \lambda_0/(4n_2)$. The total length of the N-stage, Cantor-like multilayer is $D = 2^N a + (3^N - 2^N)b$, and its optical path is $L_{opt} = 3^N(\lambda_0/4)$. The Fibonacci multilayer is constructed recursively as the binary, quasi-periodic Fibonacci sequence $S_{j+1} = S_{j-1}S_j\}$ for $j \geq 1$; with $S_0 = \{B\}$ and $S_1 = \{A\}$. It follows that $S_2 = \{BA\}$, $S_3 = \{ABA\}$, $S_4 = \{BAABA\}$, etc. and in Fig. 6c, the sequence $S_6 = \{BAABAABABAABA\}$ is shown. The layers B and A have the refractive indexes $n_1 = 2.5$ and $n_2 = 1.5$ and thicknesses a and b, respectively.
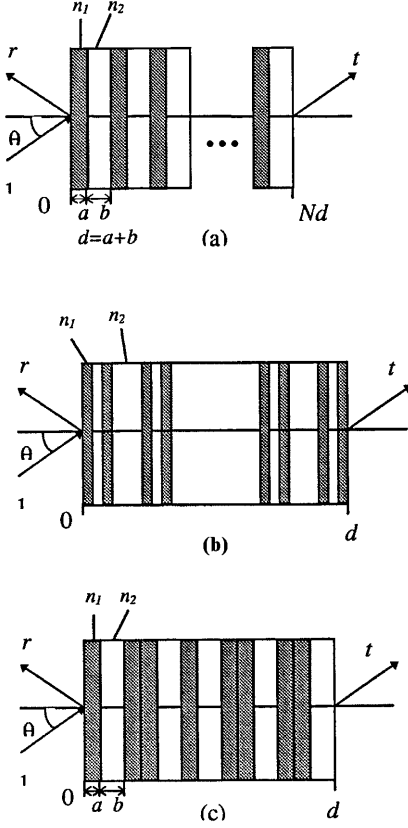
Fig. 6. Layered structures with approximately the same optical path (**a**) a periodic stack, (**b**) a Cantor sequence, (**c**) a Fibonacci sequence, $n_1 = 1.5$, $n_2 = 2.5$. $a = \lambda_0/4n_1$, $b = \lambda_0/4n_2$

The total thickness of the multilayer is given by $D_{(j+1)} = D_{(j-2)} + D_{(j-1)}$; the total optical path can be easily calculated if each layer A and B has the same optical path of one-quarter of a wavelength.

The spectral transmission characteristics T_N, the DOM ρ_N, and the dimensionless group velocity $v_N/c = (c\rho_N)^{-1}$ for the above structures are shown in Figs. 7, 8, 9. Our choice in the numbers of the Cantor prefractal level and Fibonacci sequence is somehow restricted because the total optical path L_{opt} increases as $3^N(\lambda_0/4)$ for the Cantor-like multilayer of level N; it also rapidly increases with the number J for the Fibonacci sequence. One should have a sufficiently deep band gap (obtained by using a large number of layers). On the other hand, the total number of layers should not be too large, especially if the structures are to be used for ultrashort pulses propagation, where suitable widths of resonances are required. These considerations should be taken into account considering that, as we will see below, a three-stage Cantor-like multilayer appears to be the most appropriate structure for the materials that we have chosen. Therefore, we consider the three-stage Cantor-like multilayer stack (3CS), having $L_{opt} = 6.75\lambda_0$ and total length $D = 3.79\lambda_0$, as the one for
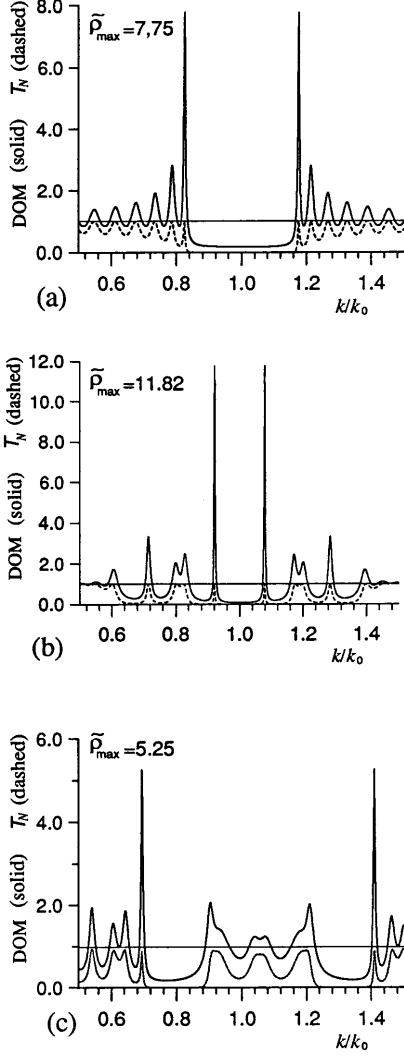
(a)

(b)

(c)

Fig. 7. The spectral transmission characteristics $T_N = |t|^2$ and the dimensionless DOM $\tilde{\rho}_N$ for normal incidence for the structure shown in Fig. 6 (**a**) for the 14-period stack (14PS), (**b**) for the 3CS, and (**c**) for the FMS8

our discussion. We compare it with a 14-periodic stack, having $L_{\mathrm{opt}} = 7\lambda_0$, $D = 3.73\lambda_0$ and with a Fibonacci multilayer S_8 (FMS8) with $L_{\mathrm{opt}} = 8.5\lambda_0$, $D = 4.8\lambda_0$ (the use of S_7 with $L_{\mathrm{opt}} = 5\lambda_0$ does not allow us to achieve sufficient depth in the band gap).

The spectral transmission characteristics $T_{\mathrm{N}} = |t|^2$ and the dimensionless DOM $\tilde{\rho}_{\mathrm{N}}$ for normal incidence are presented in Fig. 7 for (a) a 14-period stack (14PS), which has approximately the same thickness of the Cantor and Fibonacci layered structures, (b) for the 3CS, and (c) the FMS8. We have normalized the DOM for each structure considered to the dimensionless quantity $\tilde{\rho}_{\mathrm{N}} = v^{\mathrm{bulk}} \rho_{\mathrm{N}}$, as in [24], where $v^{\mathrm{bulk}} = cD/L_{\mathrm{opt}}$ represents the
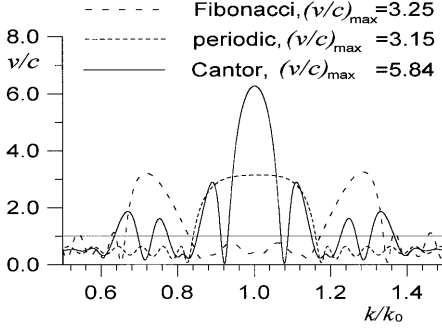
Fig. 8. The dimensionless group velocity $v_N/c = (c\rho_N)^{-1}$ for the same structures as in Fig. 6
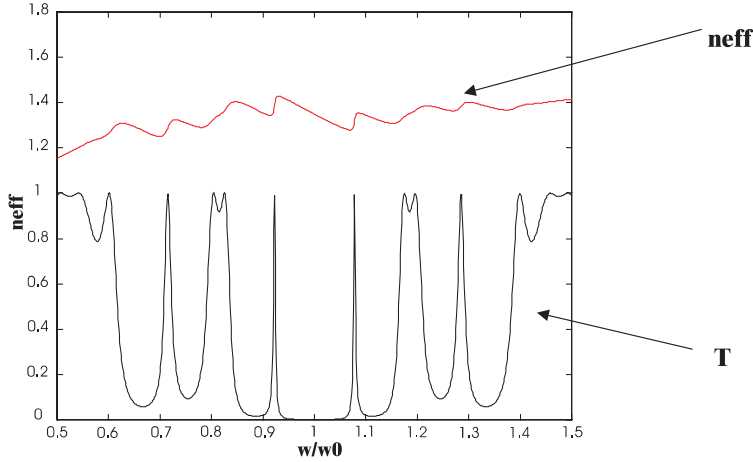

Fig. 9. Example of the behavior of the "effective index" (real part) for a Cantor set layered structure with $N = 3$, $n_1 = 1.5$, $n_2 = 2.3$, minimum optical path of $\lambda_0/4$, initiator n_2

distance D over the travel time (neglecting reflections), and c is the speed of light; this quantity is different for each structure; it is not a constant for the Cantor sequence but depends on the Cantor set level. However, for the structures that we consider, the value of v^{bulk} is approximately the same.

As we can see from Fig. 7, the 3CS has the narrowest band gap among all of the structures being considered, and the largest DOM at the band edges: it exceeds the DOM's maxima for both the periodic and Fibonacci S_8 multilayers by over 50%.

The FMS8 has the smallest maximum in the DOM; however, the transmission spectrum also exhibits two sufficiently wide band gaps within the same spectral range. This property of the Fibonacci multilayer may be compared

with the $\lambda/4 - \lambda/2$ layered structures of [24]; the location of the second-order gap is separated from the first-order gap by approximately a factor of 2, as it is for a mixed half-quarter-wave N-period stack [24]. In contrast, a factor of 3 separates the first- and the second-order band edges in both an ordinary quarter-wave N-period stack and the Cantor-like multilayer.

We may also show the behavior of the inverse Cantor-like multilayer, which means that the initiator is chosen as the material with smaller refractive index, i.e., $n_1 = 1.5$ and $n_2 = 2.5$. All of the characteristics of the inverse structure are similar to the previous ones; in this case, only a modest decrease of DOM is observed, as it is in all cases in which a weak contrast of refractive indexes exists [25].

The DOM maximum at the band edge increases proportionally to N^2 for a periodic structure, for fixed n_1 and n_2 and for a moderately large value of N [24]. A more complicated scaling law can be found for the Cantor set level: the ratio of the DOM maximum over the optical path increases approximately by a factor 2. The maximum DOM at the band edge corresponds to a "bulk localized state" inside the structure.

The dimensionless group velocity $v_N/c = (c\rho_N)^{-1}$ for the same structures of Fig. 6 is shown in Fig. 8. The group velocity within the band gap corresponds to "superluminal" tunneling velocities of a wave packet through a 1-D photonic band-gap structure [24], which was experimentally measured in [34]. In the middle of the band gap for all structures considered, there are peaks where $v_N/c > 1$. The peak for a Cantor-like structure is the largest.

We find instead a decreased group velocity at the band edge for the Cantor sequence [25] where $v/c_{\min} = 0.045$, *and the group index* $n_g = 1/0.045$, with a different shape and location compared with the periodic structure ($v/c_{\min} = 0.06$); this makes the Cantor set a good candidate for applications in the pulsed and steady-state regime.

If we increase the level of the multilayer structures, the fourth level of Cantor has optical path $L_{opt} = 20.25\lambda_0$ and $D = 12.4\lambda_0$. A 41-period stack has $L_{opt} = 20.5\lambda_0$. The peaks of transmittance are very narrow for both structures, much more so for the Cantor-like sequence. The group velocity peak inside the band gaps of a Cantor-like multilayer exceeds the group velocity for an N periodic structure by a factor of 2. At the band edge, the group velocity also decreases sharply ($v/c_{\min} = 0.0025$) for the Cantor-like multilayer (for periodic structures, the minimum value of the group velocity is $v/c_{\min} = 0.0093$).

4   Dispersive Properties of One-Dimensional Filters

Now we seek an explicit geometric dispersion relation for a multilayer, one-dimensional fractal filter of finite length; this has been proposed in [35] for periodical layered structures. The treatment is general, and it can be applied

to any kind of filter, periodic or not. Here, we report the main features of the discussion presented in [35].

We begin by writing the complex transmission coefficient for the structure, obtained via the matrix transfer method:

$$t = x + iy = \sqrt{T}e^{i\phi_t} = e^{i\varphi} , \tag{6}$$
$$\varphi = \phi_t - i \ln \sqrt{T} ,$$

where

$$\varphi_t = tg^{-1}(y/x) \pm m\pi$$

is the total phase accumulated as light propagates through the medium. The transmission $t = x + iy$ is obtained via the matrix transfer method. φ_t contains all information relating to the layered structure, such as refractive indexes, number of layers, and layer thickness. The integer m is uniquely defined by assuming that $\varphi_t(\omega)$ is a monotonically increasing function with the condition that $m = 0$ as $\omega \to 0$. This is important for calculating the effective phase of the field.

Beginning with the analogy of propagation in a homogeneous medium, we can express the total phase associated with the transmitted field as

$$\varphi = k(\omega)D = \frac{\omega}{c}n_{\text{eff}}(\omega)D , \tag{7}$$

where $k(\omega)$ is the effective wave vector; n_{eff} is therefore the effective refractive index that we attribute to the layered structure whose physical length is D. Both k and n_{eff} are complex numbers.

In particular,

$$\hat{n}_{\text{eff}}(\omega) = (c/\omega D) \left[\varphi_t - (i/2) \ln(x^2 + y^2) \right] . \tag{8}$$

Equation (8) suggests that at resonance, where $T = x^2 + y^2 = 1$, the imaginary part of the index is identically zero. Inside the gaps, where the transmission is small, scattering losses are expected to be high, leading to evanescent waves ("surface localized states"), and the imaginary part of n_{eff} is large.

We can also define the effective index as the ratio between the speed of light in vacuum and the effective phase velocity of the wave in the medium:

$$\hat{k}(\omega) = \frac{\omega}{c}\hat{n}_{\text{eff}}(\omega) . \tag{9}$$

Once the effective index has been defined, (9) represents the dispersion relation of the layered structure without any condition of periodicity. It is interesting to note that from the dispersion equation we can also define a "group index" in terms of the effective phase index as follows:

$$n_{\text{g}}(\omega) = \frac{1}{c}\frac{d\hat{k}}{d\omega} = n_{\text{eff}}(\omega) + \omega\frac{dn_{\text{eff}}}{d\omega} . \tag{10}$$

In (7) we have assumed an incident field of unit amplitude, and scattering losses are taken into account by introducing an imaginary component of the effective index of refraction. The effective index defined in (9) thus takes into account the geometric dispersion introduced by the layered structure, including the influence of entry and exit interfaces. An example of the behavior of the real part of the "effective index" for a Cantor ($N = 3$) set layered structure is shown in Fig. 9. The initiator has refractive index $n_2 = 2.3$, $n_1 = 1.4$, and the layer of minimum optical path is $\lambda_0/4$.

5   Metal–Dielectric Quasi-Periodic Filters

Recently, 1-D periodical layered structures composed of dielectric/metal layers have also been proposed (MD-PBG) [36,37,38]. In [36], a metallic multilayer arrangement in a PBG geometry has been suggested for enhancing the reflectivity with respect to bulk metal. The theoretical results showed that the reflectivity of 96% for bulk aluminum could be improved to about 98% for a layered structure. Therefore, it may be possible to arrange metals in a layered geometry to have better mirrors. It has been shown in [37,38] that it is also possible to make metals transparent to visible light and opaque to all other wavelengths of electromagnetic radiation up to UV light, even if the total metal thickness is several tens of skin-depths, or hundreds of nanometers.

The phenomenon, discussed at length in [37,38], is due to resonant tunneling of electromagnetic waves through a layered structure that may contain thin metal layers, 30–50 nm or more. By properly spacing the metal layers approximately $\lambda/2$ apart, where λ is the desired tunneling wavelength, the structure displays the following unique features: the formation of transmittance passbands, which allow visible light to propagate almost unattenuated; and the presence of a huge stop band that extends on one side to cover the entire electromagnetic spectrum down to static fields, and UV radiation on the other. For this reason, these structures have been referred to as transparent metals. The high reflectivity of the stack at low frequencies is due to the dispersive properties of the metal; the index of refraction, and hence the optical potential, becomes infinitely large, and is accurately described by the Drude model. At high frequencies, near the visible and UV range, the index of refraction of most good conductors can be of the order of unity or less. Therefore, interference may cause the formation of photonic band gap effects, i.e., the formation of passbands and frequency gaps and the effective reduction of absorption losses in the metal. Proposed applications for these structures include sensors, UV blocking films, transparent electrodes for light-emitting polymer stacks, and conductive displays, just to name a few.

In [37,38], the discussion and the examples focused on periodic metallodielectric stacks, where individual metal layer thickness varied from 10 to 40 nm. In [39], the discussion was extended to include quasi-periodic struc-

tures. It is possible to further increase the transmittance for a given amount of metal by using different geometric arrangements of metallic layers (quasi-periodic), as, for example, in Cantor or Fibonacci sets. We emphasize that the kind of interactions we are discussing can occur in an environment once thought completely inaccessible to light, i.e., through thick metal layers. For comparison, we discuss below the transmission characteristics and the density of modes for normal, TE-polarized, incident waves for periodic and quasi-periodic structures that have approximately the same total metal thickness.

The Cantor-like multilayer is generated by a metallic material having complex refractive index $\hat{n}_1$ (initiator or generator). The central part of the initiator is then replaced with a dielectric layer of refractive index $n_2 = 1.4$, according to the law of triadic Cantor construction, such that $1/3$ of the generator has the same optical path $L_{\mathrm{opt}} = \lambda_0/x$ [39], where λ_0 is the wavelength in vacuum and x is a multiple of 4, to reach a suitable dimension for the metallic layer. Thus, the generator thicknesses are $a = \lambda_0/(x\hat{n}_1)$ and $b = \lambda_0/(xn_2)$. A modified Cantor set can also be considered, in which the geometric thicknesses of the layers (and not the optical path) follow the Cantor law [39].

The Fibonacci multilayer is constructed recursively as the binary, quasi-periodic Fibonacci sequence already discussed with {B} (metallic layer) and $S_1 = \{A\}$ (dielectric layer). The layers B and A have refractive indexes n_1 and $n_2 = 1.4$ and thicknesses a and b, respectively.

As for the Cantor set, we can recursively generate the Fibonacci code by using geometric thicknesses instead of optical path lengths [39].

Our choice in the numbers of Cantor prefractal level and Fibonacci sequence is again restricted because the total optical path L_{opt} rapidly increases as $3^N(\lambda_0/x)$ for the Cantor-like multilayer of level N and also rapidly increases with the number J of the Fibonacci sequence. For simplicity, we do not change the thickness of all dielectric layers, although that may be considered an additional degree of freedom.

Depending on the desired spectral behavior, it is possible to select a suitable rule for assembling the structures. For example, large transparent spectral regions can be obtained when we use the optical path to construct a Cantor or Fibonacci code [39]. An example is given in Fig. 10, for a three-stage Cantor-like multilayer stack containing eight metallic layers, having $L/3 = \lambda_0/x(\lambda_0 = 1000\,\mathrm{nm}, x = 64)$, total length $D = 700\,\mathrm{nm}$, where the spectral transmission characteristics $T_N = t^2$ and the dimensionless DOM $\tilde{\rho}_N$ for normal incidence are presented. We observe a wide passband in the visible, and a localized weak transmission peak in the IR region ($\sim 1100\,\mathrm{nm}$), where we also calculate a high density of modes. This behavior has been found for other values of metal thickness in the Cantor code layered structure: a strong localized DOM in a region of the spectrum with low transmittivity.

Generally speaking, we remark that if the quasi-periodic sets discussed above are realized by using optical path criteria, then the band structure

Cantor N=3,
λ(rif) = 500nm
d2= 29.76 nm
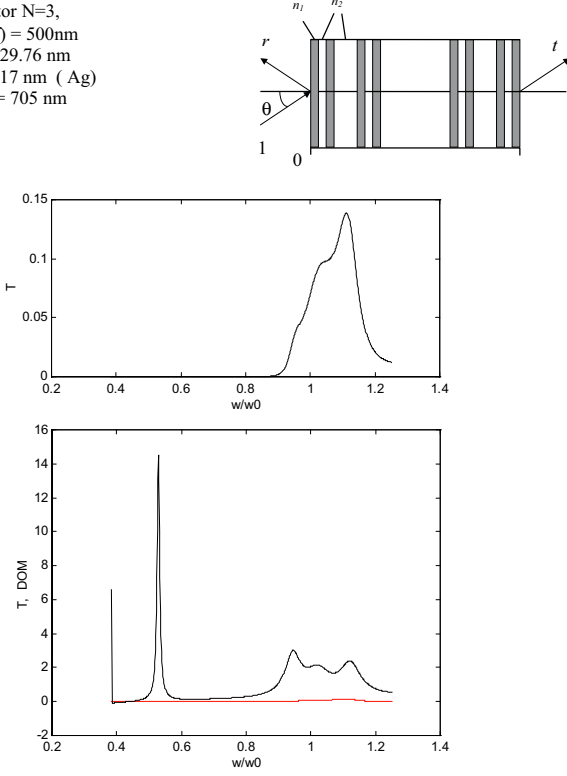d1= 17 nm (Ag)
dtot= 705 nm

Fig. 10. The spectral transmission characteristics $T_N = t^2$ and the dimensionless DOM $\tilde{\rho}_N$ for normal incidence for a three-stage Cantor-set multilayer stack containing eight metallic layers, having $L/3 = \lambda_0/x (\lambda_0 = 1000 \, \text{nm}, x = 64)$, total length $D = 700 \, \text{nm}$

achieves a different degree of complexity with sharp transmission peaks and a higher density of modes. In all of these filters, a suitable compromise between high transparency and high density of mode can be found, depending on the application. In other cases, wide passbands may be enough to satisfy device performance. So it is possible to get good transparency in the visible range even by increasing the number of metallic layer, thus making the devices practical for many applications.

6   Nonlinear Model of the Filter

One of the advantages of field localization in fractal structures is to enhance the nonlinear optical responce. This property has been discussed in [13,40] for Fibonacci quasi-periodic filters, assuming third-order nonlinear polarization in the dielectric layers. Let us discuss here the nonlinear properties of Cantor filters when a third-order nonlinear interaction is taken into account.

To describe nonlinear propagation in a multilayer structure in a steady-state regime, usually a formalism based on the nonlinear transfer matrix method [41,42,43] is applied, with the omission of spatial third harmonics generated inside each layer and of nonlinear terms in the boundary conditions. As extensively discussed in [42], the application of the nonlinear transfer formalism gives reliable results even for a high-finesse structure such as a nonlinear interferential filter, when the central spacer layer thickness exceeds the wavelength inside the material.

To take the nonlinearity into account, the refractive index of the nonlinear layers is taken as the form $n = n_{\mathrm{L}} + n_{2\mathrm{NL}}I$, where n_{L} is the linear index valid for low light intensities, $n_{2\mathrm{NL}}$ is the nonlinear coefficient of the refractive index, and I is the light intensity. We adopt the hypothesis that the electrical field in each layer is the sum of two nearly counterpropagating plane waves. Inside a single homogeneous material layer, we assume that the field is constant in amplitude but allow its phase to change nonlinearly, provided the following two conditions are fulfilled: $n_{2\mathrm{NL}}I_{\mathrm{CAV}} \ll n_{\mathrm{L}}$, and $D > \lambda_0 n_{\mathrm{L}}$, where I_{CAV} is the cavity irradiance level, D is the length of the filter, λ_0 is the incident wavelength in vacuum (in a stratified structure, the first condition has to be verified for each layer inside the structure). In what follows, we assume isotropic layers, in which the chromatic dispersion of the refractive index is taken into account.

We use the formalism described in [41,43]: the so called "transmission line theory," and we specialize it to our case of a Cantor multilayer structure that can be considered a cascade of nonlinear transmission lines. The field propagating inside the multilayer structure can be modeled by using two functions $V(z)$ and $I(z)$, proportional to the transverse components of the electrical and magnetic fields, respectively, and satisfying the following coupled differential equations:

$$\begin{cases} \frac{\mathrm{d}V}{\mathrm{d}z} = -ZI \,, \\ \frac{\mathrm{d}I}{\mathrm{d}z} = -Y_{\mathrm{NL}}V \,, \end{cases} \tag{11}$$

with $Y_{\mathrm{NL}} = Y + Y^{(3)}|V|^2$, where Z and Y_{NL} play the role of a linear impedance and nonlinear admittance, respectively, and $Y^{(3)}$ is a third-order nonlinear coefficient; Y is the unperturbed (linear) admittance per unit length. Note that $V(z)$ and $I(z)$ are reminiscent of "voltage" and "current" in a transmission line, respectively. For this reason in the following, we will refer to these quantities in that way. However, it should be understood that there are no ties to the electrical problem, and any such reference should be taken as merely suggestive. Similar arguments are valid for the parameters Z and Y_{NL} as well. It is well known that the solutions of (11) in the linear case ($Y^{(3)} = 0$) are given by

$$V(z) = a(z) + b(z) \,,$$
$$I(z) = \frac{1}{\eta}\left[a(z) - b(z)\right] \,, \tag{12}$$

where the transmission line parameters k (propagation constant) and η (characteristic impedance) are given by the following:

$$k^2 = -ZY \,,$$
$$\eta = \frac{-Z}{ik} \,.$$

Using a perturbative approach, in the nonlinear case ($Y^{(3)} \neq 0$) also, the solutions of (11) can be written as in (12), but now the forward and backward waves (a and b, respectively) are given by

$$a(z) = \hat{a}(z)e^{i\mathrm{Re}\,(k)z}$$
$$b(z) = \hat{b}(z)e^{-i\mathrm{Re}\,(k)z} \tag{13}$$

where $\hat{a}(z)$ and $\hat{b}(z)$ are not constant, but depend on the z coordinate. After substituting (12) in (11), summing and subtracting the first and the second Eq. (11), and taking into account that

$$\frac{Z}{\eta} = \eta Y = -ik \,, \tag{14}$$

we obtain the following for the forward and backward waves:

$$\frac{da}{dz} = ika - \frac{Y^{(3)}\eta}{2}|a+b|^2(a+b)$$
$$\frac{db}{dz} = -ikb + \frac{Y^{(3)}\eta}{2}|a+b|^2(a+b) \,. \tag{15}$$

Using (13) in (15), neglecting the spatial third harmonic generated inside each layer and the nonlinear term in the boundary conditions, we have the following for the slowly varying (complex) amplitudes:

$$\frac{d\hat{a}(z)}{dz} = -Im(k)\hat{a} + ik_2\left(|\hat{a}|^2 + 2\left|\hat{b}\right|^2\right)\hat{a}(z)$$
$$\frac{d\hat{b}(z)}{dz} = Im(k)\hat{b} - ik_2\left(2\left|\hat{a}\right|^2 + \left|\hat{b}\right|^2\right)\hat{b}(z) \,, \tag{16}$$

where we have introduced the nonlinear parameter

$$k_2 = k\frac{Y^{(3)}}{2Y} \,. \tag{17}$$

Note that for nonresonant nonlinearity, $Y^{(3)}$ has a pure imaginary value. It is well known that if the transmission line is lossless, Z and Y are pure imaginary parameters; as a consequence [see (13) and (17)] k, k_2 are also real parameters. It is possible to take into account losses by a complex admittance per unit length $Y = G + iW$, where G is the conductance per unit length,

responsible for the traveling wave energy loss in the transmission line. For small losses ($G \ll W$), it is possible to consider k_2 approximately real (17):

$$k_2 \cong \frac{1}{2}\mathrm{Im}\left(Y^{(3)}\right)\left|\frac{Z}{Y}\right|^{1/2}. \tag{18}$$

Considering that

$$\hat{a} = |\hat{a}|\,e^{i\varphi_a},$$
$$\hat{b} = \left|\hat{b}\right|e^{i\varphi_b}, \tag{19}$$

splitting the two (16) into their real and imaginary parts, we obtain

$$\frac{\mathrm{d}\,|\hat{a}|}{\mathrm{d}z} = -\mathrm{Im}\,(k)\,|\hat{a}|\,,$$
$$\frac{\mathrm{d}\left|\hat{b}\right|}{\mathrm{d}z} = \mathrm{Im}\,(k)\left|\hat{b}\right|, \tag{20}$$

for the magnitudes of the amplitudes $\hat{a}$ and $\hat{b}$, and

$$\frac{\mathrm{d}\varphi_a}{\mathrm{d}z} = k_2\left(|\hat{a}|^2 + 2\left|\hat{b}\right|^2\right),$$
$$\frac{\mathrm{d}\varphi_b}{\mathrm{d}z} = -k_2\left(2\,|\hat{a}|^2 + \left|\hat{b}\right|^2\right), \tag{21}$$

for the phases of the amplitudes $\hat{a}$ and $\hat{b}$. It is easy to find a general solution for (20). By subtracting the second part of (21) from the first,

$$\varphi_{\mathrm{NL}} = \varphi_a - \varphi_b = 3k_2\int_0^z \left(|\hat{a}(\zeta)|^2 + \left|\hat{b}(\zeta)\right|^2\right)d\zeta. \tag{22}$$

This result can be found in [42] for an electromagnetic plane wave propagating in a third-order nonlinear dielectric medium. From this general formalism, we specialize to the propagation along the z coordinate of a plane wave with linear polarization in the y direction. It is useful to write the complex amplitudes by two new unknown functions $\tilde{a}(z)$ and $\tilde{b}(z)$ as follows:

$$\hat{a}(z) = \tilde{a}(z)e^{-\mathrm{Im}\,(k)z}e^{i\varphi_a},$$
$$\hat{b}(z) = \tilde{b}(z)e^{\mathrm{Im}\,(k)z}e^{i\varphi_b}. \tag{23}$$

The multilayer structure can be seen as a cascade of nonlinear transmission lines. In the following, we will label with the index h the parameters of the hth transmission line. Imposing the continuity of V and I (i.e., the continuity of electrical and magnetic field tangential components) at the interface between the hth and the $(h+1)$-th transmission lines and using (23), it is possible to describe the hth transmission line by the following relation:

$$\begin{pmatrix} \tilde{a}_h \\ \tilde{b}_h \end{pmatrix} = \boldsymbol{S}_h \begin{pmatrix} \tilde{a}_{h+1} \\ \tilde{b}_{h+1} \end{pmatrix}, \tag{24}$$

where the $\boldsymbol{S}_h$ matrix, representing a two-port network, is given by

$$\boldsymbol{S}_h = \frac{e^{-i\varphi_{b_h}}}{t_h} \begin{bmatrix} e^{-i\left(k_h\delta_h+\varphi_{\mathrm{NL}_h}\right)} & r_h e^{-i\left(k_h\delta_h+\varphi_{\mathrm{NL}_h}\right)} \\ r_h e^{ik_h\delta_h} & e^{ik_h\delta_h} \end{bmatrix} \tag{25}$$

with

$$t_h = \frac{2n_h}{n_h + n_{h+1}} \, ,$$

$$r_h = \frac{n_h - n_{h+1}}{n_h + n_{h+1}} \, , \tag{26}$$

and δ_h is the length of the hth transmission line. We also assume that the nonlinearity is weak enough to neglect any reflectivity change at each interface. The input-port parameters $\tilde{a}_h, \tilde{b}_h$ are evaluated to the right of the hth interface, and the output-port parameters are evaluated to the left of the $(h+1)$-th interface. Note that the kind of multilayer structure (i.e., periodic, Cantor-like, or other) depends only on the sequence of the transmission line lengths δ_h. In this sense, the approach is applicable to any kind of layered structure.

It is easy to calculate the matrix $\boldsymbol{S}_h$ even if it depends on the port parameters for the presence of φ_{NL_h}. To do it, note that by solving (20),

$$|\hat{a}| = |\hat{a}\,(z_h)|\,e^{-\mathrm{Im}\,(k)(z-z_h)} \, ,$$

$$\left|\hat{b}\right| = \left|\hat{b}\,(z_h)\right|e^{\mathrm{Im}\,(k)(z-z_h)} \tag{27}$$

and taking into account the position (23),

$$|\tilde{a}\,(z_h)| = |\tilde{a}_h| = |\hat{a}\,(z_h)| \, ,$$

$$\left|\tilde{b}_h\,(z_h)\right| = \left|\tilde{b}_h\right| = \left|\hat{b}\,(z_h)\right| \, . \tag{28}$$

So, according to (20), (22) becomes

$$\varphi_{\mathrm{NL}_h} = 3k_{2_h}\left[|\tilde{a}_h|^2\,\frac{1-e^{-2\mathrm{Im}\,(k_h)\delta_h}}{2\mathrm{Im}\,(k_h)} + \left|\tilde{b}_h\right|^2\,\frac{e^{2\mathrm{Im}\,(k_h)\delta_h}-1}{2\mathrm{Im}\,(k_h)}\right] \, . \tag{29}$$

It is necessary to know the magnitude of the input-port parameters to calculate the phase shift (29). From (24) and (25),

$$|\tilde{a}_h| = \frac{1}{|t_h|}\left|e^{-ik_h\delta_h}\tilde{a}_{h+1} + r_h e^{-ik_h\delta_h}\tilde{b}_{h+1}\right| \, ,$$

$$\left|\tilde{b}_h\right| = \frac{1}{|t_h|}\left|r_h e^{ik_h\delta_h}\tilde{a}_{h+1} + e^{ik_h\delta_h}\tilde{b}_{h+1}\right| \, . \tag{30}$$

This means that $|\tilde{a}_h|$ and $\left|\tilde{b}_h\right|$ can be found by using the matrix $\boldsymbol{S}_h$ as if the nonlinearity did not exist at all ($\varphi_{\mathrm{NL}_h} = 0$). Because we consider that the layered structure is modeled by a cascade of p two-port networks, it is possible

to calculate the port parameters of the network $p, p-1, \ldots, 1$, once $\tilde{a}_{p+1}$ and $\tilde{b}_{p+1}$ are known. The procedure we use is as follows (the so called "dummy" method [42]). We consider a given transmitted field, hence we determine the incident and reflected amplitudes just inside the output interface, provided that the linear refractive indexes are used in the calculation. Then from the nonlinear propagation, we determine the fields across the final layer. We use these fields to determine the total phase change across the final layer in the presence of the nonlinearity. Hence, we determine the forward and backward fields at the penultimate interface. We iterate this procedure until the incident field is calculated.

When the multilayer structure is made with lossless dielectric layers, so that the propagation constants of the fields are purely real ($\mathrm{Im}\,(k) = 0$), $n_{2\mathrm{nl}}$ is the Kerr coefficient

$$n_{2\mathrm{nl}} = \frac{\chi^{(3)}}{2n_h}$$

$$\left(n_{2\mathrm{nl}} = \frac{1}{2}\varepsilon_0 c n_h n_{2_h}^{\mathrm{nl}} \right). \tag{31}$$

It is useful to normalize the intensities to the value

$$I_b = \frac{1}{|n_{2\mathrm{nl}}|}. \tag{32}$$

When losses are taken into account, the following normalization is useful instead:

$$I_b^\alpha = \frac{\alpha}{k_0\,|n_{2\mathrm{nl}}|}. \tag{33}$$

Because the effective intensity in each layer is defined as

$$I_{\mathrm{eff}_h} = \varepsilon_0 c n_h \left[|\tilde{a}_h|^2\, \frac{1 - \mathrm{e}^{-2\mathrm{Im}\,(k_h)\delta_h}}{2\mathrm{Im}\,(k_h)} + \left|\tilde{b}_h\right|^2\, \frac{\mathrm{e}^{2\mathrm{Im}\,(k_h)\delta_h} - 1}{3\mathrm{Im}\,(k_h)} \right], \tag{34}$$

the nonlinear phase shift (29) can be written for the lossless case as

$$\varphi_{\mathrm{NL}_h} = 3k_0\delta_h\, \frac{n_{2_h}^{\mathrm{nl}}}{\varepsilon_0 c n_h}\, I_{\mathrm{eff}_h}, \tag{35}$$

where I_{eff_h} is the normalized effective intensity of the hth transmission line.

When losses are taken into account,

$$\varphi_{\mathrm{NL}_h} = 3k_0\, \frac{n_{2_h}^{\mathrm{nl}}}{\alpha_h \varepsilon_0 c n_h}\, I_{\mathrm{eff}_h}. \tag{36}$$

Moreover, we set as incident and transmitted input, respectively,

$$I_{\mathrm{i}} = 1/2\varepsilon_0 c n_0\, |\hat{a}_0|^2,$$

$$I_{\mathrm{t}} = 1/2\varepsilon_0 c n_{p+1}\, |\hat{a}_{p+1}|^2. \tag{37}$$

When the local intensity is very low, the effect of the nonlinear phase change on the forward and backward component of the fields is negligible with respect to the linear phase shift in each layer. To highlight nonlinear effects on the transmission spectrum, let us consider a Cantor filter $N = 3$ realized with $AlAs/Al_{0.3} GaAS_{0.7}$, (the initiator is the AlAs layer), where the minimum optical path is $\lambda/4$, with $\lambda = 1.06\,\mu m$. A negative nonlinear refractive index has been considered for wavelengths around $1.06\,\mu m$ of the order of $- 4 \times 10^{-13}\,cm^2/\,W$, and no dispersion of the nonlinear coefficient has been taken into account. A nonlinear spectral shift is found for an input intensity of $10^{10}\,W/\,cm^2$ (see Fig. 11). The frequency shift of the nonlinear spectrum is strongly influenced by the refractive index of the initiator (high or low refractive index) and by the refractive index contrast among the constituent layers. The change of the shift, if toward higher or lower frequencies, depends on the sign of the nonlinear contribution [44]. Examples of nonlinear transmission for fixed spectral values are given in Fig. 12. An example of output versus input intensity is shown for the level $N = 2$ (Fig. 12a), and $N = 3$ (Fig. 12c). The corresponding spectral positions are shown in Fig. 12b and Fig. 12d. In this example, a positive nonlinearity of thermal origin has been considered. A more detailed discussion is presented in [26,33] where a comparison has also been made with a traditional layered structure. A reduction of the input threshold intensity for bistability was found. Multistable behavior can also occur, depending on the various system parameters and materials at our disposal.
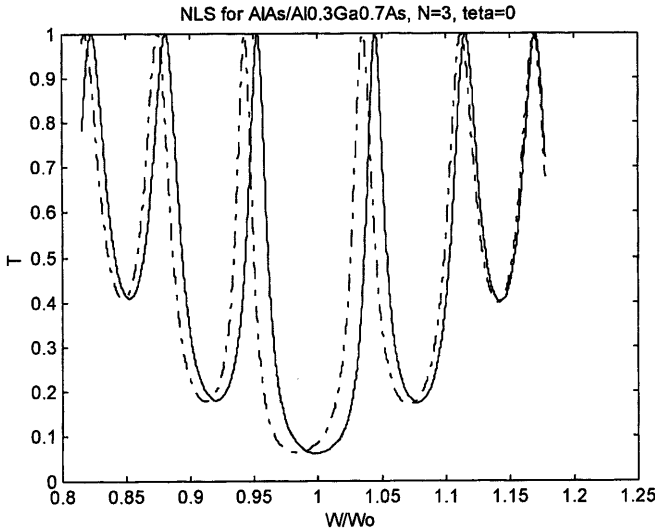

Fig. 11. Cantor filter with $N = 3$ realized with $AlAs/Al_{0.3} GaAS_{0.7}$, (the initiator is the AlAs layer); the minimum optical path is $\lambda/4$, with $\lambda = 1.06\,\mu m$: *continuous line*: linear spectrum; *dotted line*: nonlinear spectrum at $10^{10}\,W/cm^2$
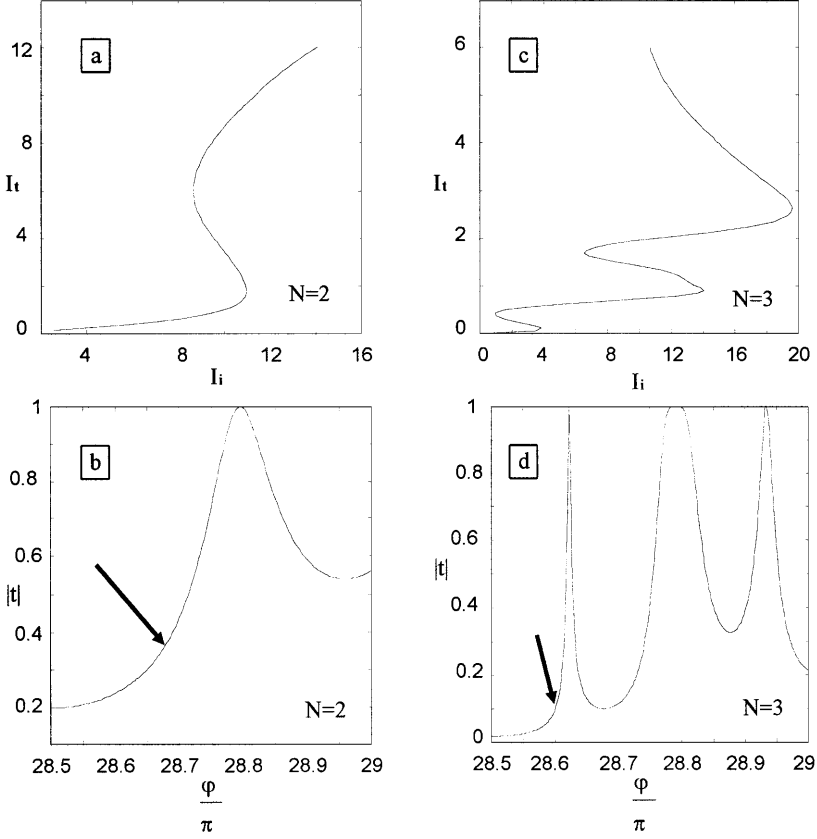
Fig. 12. Output (I_t) vs input (I_i) intensity (arbitrary units) for the level $N = 2$ (**a**), and $N = 3$ (**c**) of a Cantor structure. The corresponding spectral positions are shown in (**b**) and (**d**). Refractive indexes are $n_1 = 1.4$, $n_2 = 2.3$. Thermal nonlinearity has been taken into account for the highest refractive index layer, which induces a nonlinear refractive index change of 5×10^{-2} when the bistability threshold is reached

The same concepts discussed for multilayers structures can be translated in the form of guided wave geometry, where a quasi-periodic corrugation is "written" on the top of the guide [43]. All of these properties make nonlinear, quasi-periodic structures very interesting for nonlinear filtering properties and applications.

7   Mesoscopic Layered Structures

In a stratified structure, the fields inside the structure must be determined by solving a set of transfer-matrix equations. Such an approach is necessary if the layer thicknesses are of the order of the incident wavelength, because

interference effects then become important. If individual layer thicknesses are much less than the incident wavelength, the multilayer structure can be considered a uniform effective medium. It is then possible to introduce some simplifying considerations into all calculations of the optical properties of the layers. In fact, in this case the propagation of the light through the structure can be described in terms of effective linear and nonlinear optical susceptibilities.

We assume that the thickness of each layer [28] is much larger than an atomic dimension, but much smaller than the incident wavelength. Results of the analysis depend critically on the polarization of the incident beam. In particular, if the electrical field is TE polarized, then it is spatially uniform within the composite material (because of the boundary condition that states that the tangential component of the electrical field must be continuous at an interface); consequently, the optical constants of the composite [28] become simple averages of those of the constituent materials.

On the other hand, if the incident electrical field is polarized TM, then the electrical field becomes nonuniformly distributed inside the layers of the composite, and, taking advantage of boundary conditions at each layer, the effective linear optical constant is given by [28]

$$\frac{1}{n_{\text{eff}}^2} = \frac{f_a}{n_a^2} + \frac{f_b}{n_b^2} \, . \tag{38}$$

If we have a periodic layered distribution, the volume fraction f_a and f_b of each material is given by

$$f_a = \frac{d_{\text{tot}}|_a}{d_{\text{tot}}}$$

$$f_b = \frac{d_{\text{tot}}|_b}{d_{\text{tot}}} \, , \tag{39}$$

where d_{tot} is the total thickness of the structure and $d_{\text{tot}}|_j (j = a, b)$ is the total thickness of the structure if the initiator is the material a or b. If a triadic Cantor structure is considered, then the volume fractions f_a and f_b of each material are given by

$$f_a = \frac{d_{\text{tot}}|_a}{d_{\text{tot}}} = \frac{2^N d_a}{2^N d_a + (3^N - 2^N)d_b} \, ,$$

$$f_b = \frac{(3^N - 2^N)d_b}{(3^N - 2^N)d_b + 2^N d_a} \, . \tag{40}$$

where d_a and d_b are the thicknesses of the smallest layers of the structure. We observe that we have an additional parameter, compared with a periodic structure, that is, the Cantor level N.

The layering produces a large enhancement of the effective refractive index. An example is given in Fig. 13a, where the ratio n_{eff}/n_a is shown for
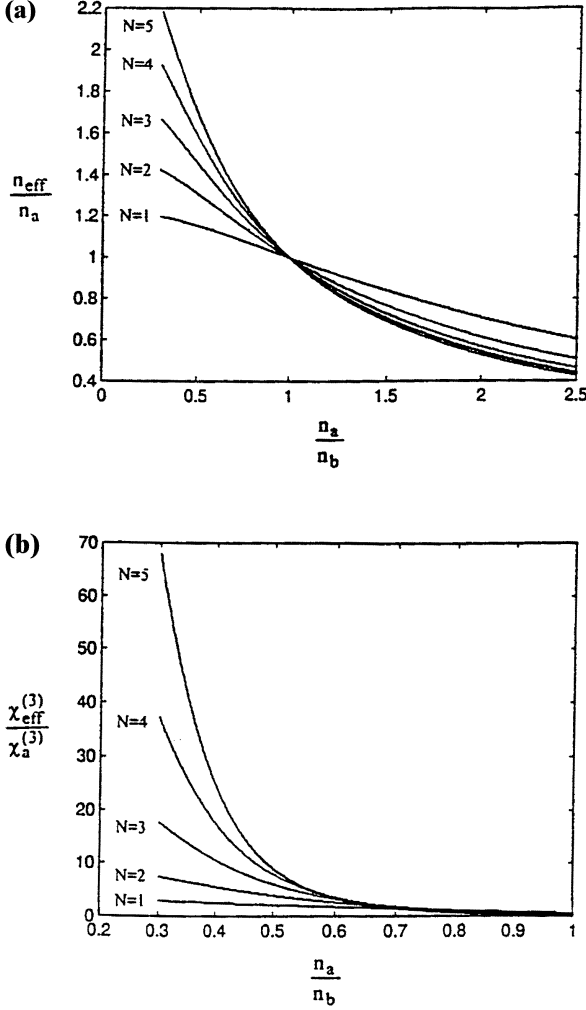
Fig. 13. Enhancement of the effective refractive index in the mesoscopic approximation: (**a**) the ratio n_{eff}/n_a is presented for several values of the Cantor level as a function of $n_a(\omega)/n_b(\omega)$; (**b**) third-order nonlinear susceptibility

several values of the Cantor level as a function of $n_a(\omega)/n_b(\omega)$. In this example, the multilayer is realized with two different materials whose optical path follows the triadic Cantor code. The same can be done with a Fibonacci code, as discussed in [28], where it is shown that an enhancement of the effective index is found when a nonlinear material is taken into account in one of the layers constituting the structure.

The effective index model in the mesoscopic limit, i.e., no interference of the field inside the structure, can show the same value of the "interferometric"

effective index, as discussed in Sect. 4, and where it has been evaluated from the transmission properties of the layered structure. This is possible when very low refractive index contrast among the layers is considered in the limit of long wavelengths. An example of the behavior is shown in Fig. 14, where the difference among the two "effective indexes" is reported for several values of the refractive index contrast. Therefore the "interferometric" effective index admits the mesoscopic effective index as a limiting value.

Quasi-periodic layered structures enhance the nonlinear susceptibility of a periodic structure [28]. Again we will consider the fractal structures realized by following a triadic Cantor sequence or a Fibonacci sequence, alternating layers of two different materials (a, b) possessing linear refractive indexes n_a and n_b and nonlinear susceptibilities (we suppose only third-order nonlinearity) χ_a^{NL} and χ_b^{NL}, respectively. The two constituent materials are assumed to be lossless, and the response time of the composite is essentially the same as that of the nonlinear constituent. We assume that each layer is thicker than an atomic dimension but much smaller than the incident wavelength. Consequently, the structural properties of each constituent material are essentially the same as those of a bulk sample, but the propagation of light through the structure can be described in terms of effective linear and nonlinear optical susceptibilities. By using the same notation given in (33) and (34), for TM polarization, the nonlinear effective susceptibility is

$$\chi_{\mathrm{eff}}^{(2)}(\omega = \omega + \omega - \omega) = \frac{\frac{f_a \chi_a^{(3)}}{|n_a^2(\omega)|^2 n_a^4(\omega)} + \frac{f_b \chi_b^{(3)}}{\left|n_b^2(\omega)\right|^2 n_b^4(\omega)}}{\left[\frac{f_a}{n_a^2(\omega)} + \frac{f_b}{n_b^2(\omega)}\right]^2 \left[\frac{f_a}{n_a^2(\omega)} + \frac{f_b}{n_b^2(\omega)}\right]^2} . \tag{41}$$
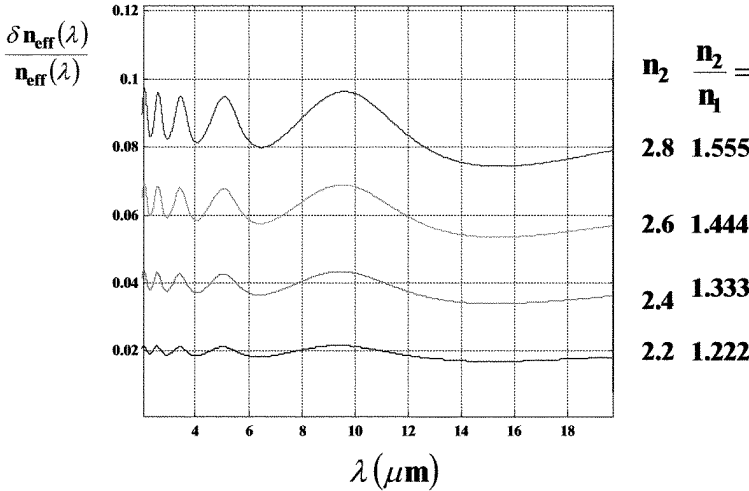

Fig. 14. The difference between the "interferometric" and "mesoscopic" effective index reported for several values of the refractive index contrast

Then, for the quasi-periodic Cantor structure, the nonlinear effective refractive index may be much higher than that of the corresponding periodic structure (see Fig. 13b), depending on the material selected as the initiator and, for the Cantor code, from the level of the iteration. Among the quasi-periodic structures studied in [28], a greater enhancement of the Cantor sequence with respect to the Fibonacci sequence can be obtained, on the Cantor level and on the Fibonacci sequence, depending on which material is used as the initiator of the Cantor sequence.

The Fibonacci structure presents an enhancement of the optical constants which is independent of the level of the sequence used [28].

8   Conclusions

Fractal layered composites exhibit very interesting and flexible properties. We have discussed here 1-D layered structures following Cantor and Fibonacci fractal codes. The Cantor layered structures offer greater flexibility in handling spectral transmission compared to periodic structures, which may turn out particularly useful for unique filtering properties, mainly when the nonlinear response of the structure is taken into account. The Fibonacci fractal code also has some advantage, even if somehow less interesting than the Cantor code. In the nonlinear case, the enhancement of field localization resulting from the fractal nature may be very usefully exploited in nonlinear optical applications.

Mesoscopic treatment of the structures can be performed when their thickness is much smaller than the incident wavelength, giving rise to interesting enhancements of the linear and nonlinear effective refractive indexes. Finally, we want to point out that the general methods outlined in this review can be very easily applied to other fractal codes.

Acknowledgments

References

1. R. Merlin, Structural and electronic properties of nonperiodic superlattices, IEEE J. Quant. Electron. **24**, 1791 (1988)   63
2. S. A. Gradesluk, V. Freilikher, Localization and wave propagation in randomly layered media, Sov. Phys. Uspekhi **33**, 134 (1990)   63
3. M. Kohmoto, L. P. Kadanoff, C. Tang, Localization Problem in One Dimension: Mapping and Escape, Phys. Rev. Lett. **50**, 1870 (1983)   63
4. M. Kohmoto, B. Sutherland, C. Tang, Critical wave functions and a Cantor-set spectrum of a one-dimensional quasicrystal model, Phys. Rev. B **35**, 1020 (1987)   63

5. D. Shechtman, J. Black, D. Gratias, J. W. Cahn, Metallic Phase with Long-Range Orientational Order and No Translational Symmetry, Phys. Rev. Lett **53**, 1951 (1984) 63

6. R. Merlin, K. Bajima, R. Clarke, F. T. Juang, P. K. Bhatacharyya, Quasi-periodic GaAs-AlAs Heterostructures, Phys. Rev. Lett. **55,** 1768 (1986) 63, 64

7. M. Kohmoto, B. Sutherland, K. Iguchi, Localization in Optics, Quasi-periodic media, Phys. Rev. Lett. **58**, 2436 (1987) 63, 64

8. L. Gourley, C. P. Tiggs, R. P. Schneider, Jr., T. M. Brennan, B. E. Hammons, A. E. McDonald, Optical properties of fractal quantum wells, Appl. Phys. Lett. **62**, 1736 (1993) 64

9. O. V. Angelsky, P. P. Maksimyak, T. O. Perun, Dimensionality in optical fields and signals, Appl. Opt. **32**, 6066 (1993) 64

10. M. Bertolotti, P. Masciulli, C. Sibilia, Spectral transmission properties of a self-similar optical Fabry-Perot resonator, Opt. Lett. **19**, 777 (1994) 64, 65, 67

11. Rammal, G. Toulouse, Random walks on fractal structures and percolation clusters, Phys. Lett. **44**, 412 (1983) 64

12. F. Craciun, A. Bettucci, E. Molinari, A. Petri, A. Alippi, Direct experimental observation of fracton mode patterns in one dimensional Cantor composite, Phys. Rev. Lett. **68**, 342 (1992) 64

13. S. Dutta Gupta, D. S. Ray, Localization problem in optics: Nonlinear quasi-periodic media, Phy. Rev. B **41**, 8047 (1990) 64, 66, 78

14. Y. Sakurada, J. Uozumi, T. Asakura, Fresnel diffraction by one-dimensional regular fractals, Pure Appl. Opt. **1**, 29 (1992) 64

15. M. V. Berry, Diffractals, J. Phys. A **12**, 781 (1979) 64

16. J. Uozumi, T. Asakura, Fractal Optics, Curr. Trends Opt. **6**, 83 (1994) 64

17. C. Allain, M. Cloitre, Optical diffraction on fractals, Phys. Rev. B **33**, 3566 (1986) 64

18. D. A. Zimnyakov, V. V. Tuchin, Scale properties of the diffraction fields induced by pre-fractal random screens, in *Fractal Frontiers*, M. M. Novak, T. G. Dewey (Eds.) (World Scientific, Singapore 1997) pp. 281–290 64

19. J. M. Elson, J. M. Bennett, Relation between the angular dependence of scattering and the statistical properties of optical surfaces, J. Opt. Soc. Am. **69**, 31 (1979) 64

20. J. D. Joannopulos, P. R. Villeneuve, S. Fan, Putting a new twist on light, Nature **386**, 143 (1997) 64

21. E. Yablonovich, Inhibited spontaneous emission in solid-state physics and electronics, Phys. Rev. Lett. **58**, 2059 (1987) 64

22. W. Robertson, Measurement of photonic band structures in a two-dimensional periodic dielectric array, Phys. Rev. Lett. **68**, 2023 (1992) 64

23. M. Scalora, J. P. Dowling, C. M. Bowden, M. J. Bloemer, Optical limiting and switching of ultrashort pulses in Nonlinear PBG Materials, Phys. Rev. Lett. **73**, 136 (1994) 64

24. J. M. Bendickson, J. P. Dowling, M. Scalora, Analytic expression for electromagnetic mode density of finite 1-D PBG structures, Phys. Rev. E **53**, 4107 (1996) 64, 70, 72, 74

25. C. Sibilia, I. Nefedov, M. Scalora, M. Bertolotti, Electromagnetic mode density for finite quasi-periodic structures, J. Opt. Soc. Am. B **15**, 1947 (1998) 64, 70, 74

26. M. Bertolotti, P. Masciulli, P. Ranieri, C. Sibilia, Optical bistability in a nonlinear Cantor corrugated waveguide, J. Opt. Soc. Am. B **13**, 1512 (1996) 64, 84

27. M. Bertolotti, P. Masciulli, C. Sibilia, F. Wijnands, H. Hoekstra, Transmission properties of A Cantor corrugated waveguide, J. Opt. Soc. Am. B **13**, 628 (1996) 64

28. C. Sibilia, F. Tropea, M. Bertolotti, Enhanced nonlinear optical response of a Cantor-like and Fibonacci-like quasi-periodic structures, J. Mod. Opt. **45**, 2255 (1998) 64, 86, 87, 88, 89

29. B. B. Mandelbrot, *The Fractal Geometry of Nature* (Freeman, San Francisco 1992) 64

30. P. de Vries, H. De Raedt, A. Lagendijk, Localization of waves in fractals: spatial behaviour, Phys. Rev. Lett. **62**, 2515 (1989) 66

31. Badgasaryan, C. Sibilia, Proc. COST 240 (Springer, Berlin, Heidelberg 1999) 66

32. W. Gellerman, M. Kohmoto, B. Sutherland, P. C. Taylor, Localization of light waves in Fibonacci dielectric multilayers, Phys. Rev. Lett. **72**, 633 (1994) 66

33. M. Bertolotti, C. Sibilia, Optical properties of quasiperiodic structures: Linear and nonlinear analysis, Springer Ser. Opt. Sci. **74**, 258 (2000) 70, 84

34. A. M. Steinberg, R. Y. Chiao, Subfemtosecond determination of transmission delay times for a dielectric mirror (photonic band gap) as a junction of the angle of incidence, Phys. Rev. A **51**, 3525 (1995) 74

35. M. Centini, C. Sibilia, M. Scalora, G. D'Aguanno, M. Bertolotti, I. Nefedov, M. Bloemer, C. Bowden, Dispersive properties of finite, one-dimensional photonic band gap structures: Applications to nonlinear quadratic interactions, Phys. Rev. E **56**, 4891 (1999) 74, 75

36. A. J. Ward, J. B. Pendry, W. J. Stewart, Photonic dispersion surfaces, J. Phys. Cond. Matter **7**, 2217 (1995) 76

37. M. Scalora, M. J. Bloemer, A. S. Pethel, J. P. Dowling, C. M. Bowden, A. S. Manka, Transparent, metallo-dielectric, one-dimensional, photonic band-gap structures, J. Appl. Phys. **83** 2377 (1998) 76

38. M. J. Bloemer, M. Scalora, Transmissive properties of Ag/MgF2 photonic band gaps, Appl. Phys. Lett. **72**, 1676 (1998) 76

39. C. Sibilia, M. Scalora, M. Centini, M. Bertolotti, M. J. Bloemer, C. Bowden, Electromagnetic properties of periodic and quasi periodic one-dimensional metallo-dielectric photonic band gap structures, Pure Appl. Optics **1**, 490 (1999) 76, 77

40. S. Dutta Gupta, Nonlinear Optics of Stratified Media, Prog. Opt. **XXXVIII**, 1 (1998) 78

41. L. Caleo, C. Sibilia, P. Masciulli, M. Bertolotti, Nonlinear optical filters based on the cascading second order effect, J. Opt. Soc. Am. B **14**, 2315 (1997) 79

42. J. Danckaert, K. Fobelets, I. Veretennicoff, G. Vitrant, R. Reinish, Dispersive optical bistability in stratified structures, Phys. Rev. B **44**, 8214 (1991) 79, 81, 83

43. M. Bertolotti, P. Masciulli, P. Ranieri, C. Sibilia, J. Opt. Soc. Am. B**13**, 1517 (1996) 79, 85

44. C. Sibilia, F. Tropea, M. Bertolotti, V. Rusu, I. Grave, Nonlinear optical properties of Cantor-like quasiperiodic filters, to be published 84

Index